PERGAMON

Journal of Structural Geology 21 (1999) 1623–1636

JOURNAL OF STRUCTURAL GEOLOGY

www.elsevier.nl/locate/jstrugeo

Fault propagation and segmentation: insight from the microstructural examination of a small fault

Jan M. Vermilye*, [1], Christopher H. Scholz

Lamont–Doherty Earth Observatory, Columbia University, Palisades, NY 10964, USA

Received 2 December 1997; accepted 12 May 1999

Abstract

Naturally formed faults typically are segmented. The detailed microstructural examination of a small brittle fault in the Shawangunk Mountains of Ulster County, New York provides new insight into the segmentation process. In brittle faulting the propagation directions of faults can be determined from the orientations of microfractures formed within the process zone. We have determined the propagation directions at several locations along this strike-slip fault and these directions indicate growth of individual segments from the segment centers toward the tips. This information, combined with observed fault geometry, allows us to reconstruct a plausible growth history of this segmented fault and of the formation of the segment boundaries. © 1999 Elsevier Science Ltd. All rights reserved.

1. Introduction

Observations of faults within the brittle field reveal them to be complex systems, consisting of segments displaying varying degrees of connectedness (e.g. Segall and Pollard, 1980, 1983; Martel et al., 1988; Peacock, 1991; Peacock and Sanderson, 1991, 1994; Anders and Schlische, 1994; Trudgill and Cartwright, 1994; Cartwright et al., 1995; Dawers and Anders, 1995). Although stress interactions between fault segments have been modeled (e.g. Segall and Pollard, 1980; Burgmann and Pollard, 1994; Burgmann et al., 1994) and segment boundaries have been examined in the field (Martel et al., 1988; Anders and Schlische, 1994; Cartwright et al., 1995; Huggins et al., 1995) the processes by which segments form are still poorly understood. Fault segmentation (the observed segmented geometry) may result from linkage of pre-existing segments or from the breakdown of a larger pre-existing structure.

Fault growth produces two deformation zones: a fault core composed of slip surfaces and comminuted rock material, and a broader volume of more distributed deformation, known as the damage zone (Caine et al., 1996). These two deformation zones record complementary evidence of fault growth. Observations of these deformation zones combined with observations of segment boundary geometry, may allow reconstruction of the manner in which the segments formed.

Investigations of fault growth commonly utilize shear cracks to model faults (e.g. Segall and Pollard, 1980; Cowie and Scholz, 1992; Scholz et al., 1993). While cracks (idealized, elastic discontinuities) differ significantly from faults (structural discontinuities in rock, with displacements parallel to the discontinuities) the stress fields associated with shear cracks and faults are similar (Engelder et al., 1993). Physically realistic models for fault growth must address the laboratory observation that faults, unlike cracks, do not grow by simple propagation within the fracture plane but form by a more complicated breakdown process. In brittle rock this process consists of shear plane growth resulting from the coalescence of opening-mode microfractures (Scholz, 1968; Hallbauer et al., 1973; Cox and Scholz, 1988a, 1988b; Lockner et al., 1991, 1992; Vermilye and Scholz, 1998).

* Corresponding author.
E-mail address: janv@ldeo.columbia.edu (J.M. Vermilye)
[1] Now at: Whittier College, Department of Earth and Environmental Science, Whittier, CA 90608, USA.

PII: S0191-8141(99)00093-0

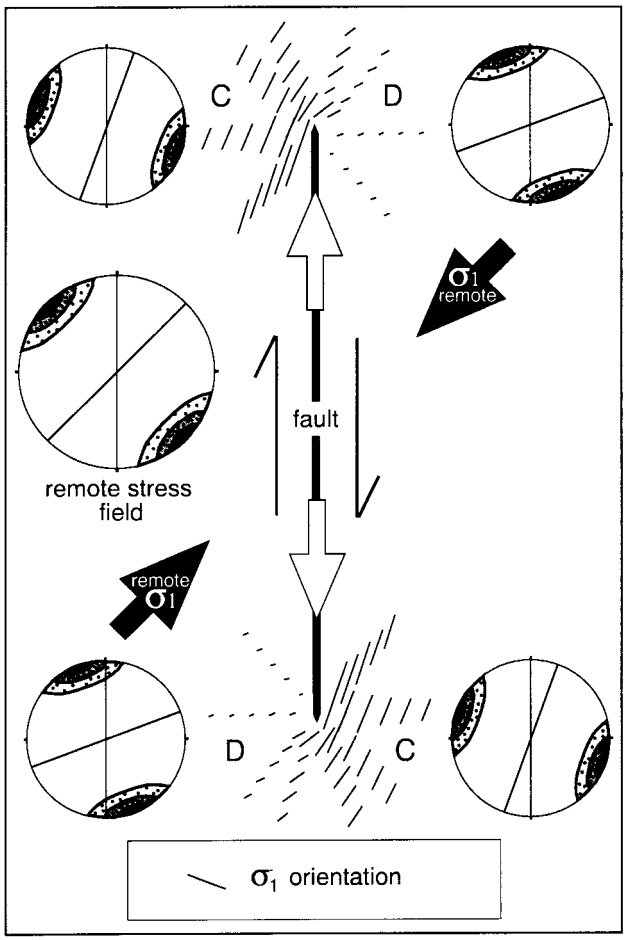

Fig. 1. Plot of the calculated maximum compressive stress (σ_1) surrounding the tips of a mode II crack, showing rotation to lower angles with the fault in the compressive quadrants (C) and higher angles in the dilational quadrants (D). Solid arrows = remote σ_1 and open arrows = crack propagation direction. The small lines indicate orientation and magnitude (proportional to length) of the altered σ_1. In each quadrant, the stereoplots show idealized plots of expected poles to microfractures and the plane representing the maximum concentration. The central stereoplot represents the remote stress field (see text for parameters of calculations; after Vermilye and Scholz, 1998).

The zone of microfracturing directly associated with this shear plane growth is defined as the process zone (e.g. Friedman et al., 1972; Ingraffea, 1987; Reches and Lockner, 1994; Vermilye and Scholz, 1998). Process zone microfractures form in a volume of rock surrounding the fault tip, and as the fault grows they are left in a wake behind the propagating tip. This results in a continuous process zone surrounding the fault core (Vermilye and Scholz, 1998). Since opening-mode microfractures grow in length parallel to the maximum compressive stress (σ_1) and dilate parallel to the least compressive stress (σ_3) their orientations are good indicators of the local principal stress directions. As such, the orientations of microfractures formed within the process zone record a representation of the passage of the crack tip stress field (Vermilye and Scholz, 1998).

Local alterations in stress fields, caused by fault propagation, may result in asymmetrical distributions of process zone microfracture populations (Scholz et al., 1993; Anders and Wiltschko, 1994; Moore and Lockner, 1995; Vermilye and Scholz, 1998). For a mode II (sliding, shear displacement) crack the remote maximum compressive stress is rotated in the vicinity of the crack tip to make lower angles with the fracture plane in the compressive quadrants and higher angles in the tensile quadrants (Fig. 1). This results in an asymmetry of stresses across the crack plane. The sense of asymmetry is dependent not only on the sense of slip but also on the direction of propagation of the crack tip past the point of observation. For right-lateral displacement, the principal stresses and associated maximum microfracture concentration will be rotated to higher angles on the right-hand side of the crack and to lower angles on the left-hand side of the crack, when looking in the direction of propagation. The stress orientations shown in Fig. 1 are computed in Scholz et al. (1993), utilizing the stress limit from the Cowie and Scholz fault growth model (Cowie and Scholz, 1992), the elastic solution for the near-field crack tip stress field (e.g. Lawn and Wilshaw, 1975), and an empirical dilatancy-stress function (e.g. Scholz, 1968). The assumption is made that cracking will occur at all points where stresses exceed the critical dilatancy stress. Cumulative microfracture density, representing passage of the fault tip at any given distance perpendicular to the fault, is estimated by integration of the entire fault tip stress field, parallel to the fault at that distance, and multiplying the maximum stress by the empirical dilatancy-stress function. These computations predict a logarithmic decay in microfracture density as a function of perpendicular distance from the fault surface. The asymmetry of stress orientations is accompanied by an asymmetry of least compressive stress magnitude, with higher tensile stresses in the tensile quadrants. This leads to higher microfracture densities in the tensile quadrants. Such asymmetrical microfracture populations are referred to as a mode II signature and they allow determination of the propagation direction for mode II faults (Vermilye and Scholz, 1998).

While the orientation of the stress field for a propagating mode II crack is asymmetric across the fracture plane, the orientation of stresses for mode I and mode III cracks are symmetric. Consequently, one cannot discriminate the propagation direction for these modes with observations of microfracture orientations. For all modes the ambient remote stress is greatly amplified near the crack tip and passage of the tip with these higher stresses is expected to generate a process

zone which remains as a wake behind the propagating tip (e.g. Pollard and Segall, 1987; Vermilye and Scholz, 1998). It is reasonable to expect that the highest stresses a rock might experience would be in the vicinity of the fault tip, just prior to failure and that damage produced by this stress concentration might outweigh damage resulting from subsequent slip on the fault. Fault growth in laboratory experiments has produced just such process zone wakes, with the predicted propagation directions confirmed with acoustic emission events (Lockner et al., 1992; Reches and Lockner, 1994; Moore and Lockner, 1995).

As slip increases on a shear plane, a layer of fine-grained gouge or cataclasite can form. This fault core material (Caine et al., 1996) consists of accumulated detritus resulting from frictional wear associated with slip on the fault surface. Since thickness of the gouge zone generally increases with displacement on the fault (Scholz, 1987; Hull, 1988), by analogy we might expect an increase in the thickness of the core as slip increases from the tip toward the center of a fault segment. If this is the case, the location of maximum core thickness might indicate the location of slip initiation. This provides complimentary information which can be used to verify propagation directions determined by examination of the process zone.

This study presents observations of the process zone and the fault core associated with a segmented brittle fault. The process zone microfracture orientations are used to determine the propagation directions associated with growth of the segments. We relate the changes in propagation direction, variability in fault core thickness and fault plane location within the core to fault segmentation and propose a plausible model for growth of the segments.

2. Geology

The Shawangunk Mountains are the northeastern-most expression of the Valley and Ridge province of the central Appalachians. The Paleozoic strata display broad open folds, northeast-striking thrust faults and a conjugate set of steeply dipping strike-slip faults, all of which developed in Alleghanian time (Epstein and Lyttle, 1987). This manuscript presents detailed observations of one of these small strike-slip faults. Cross-cutting relations between the thrusts and strike-slip faults indicate that they are coeval. The depth of faulting, estimated from the thickness of overlying strata, is 6–8 km (Berkey, 1911; Beaumont et al., 1987) for an Alleghanian age of deformation. This depth is consistent with fluid inclusion analysis of syn-faulting quartz and sphalerite vein deposits, indicating that temperatures were between 120 and 260°C at the time of faulting (Wilbur, 1986; Wilbur et al., 1990). Fission-track analysis of apatite and zircon grains in the overlying strata (Lakatos and Miller, 1983) also suggest a burial depth of 7 km and a temperature of about 260°C.

The mountains are capped by the Middle Silurian-aged Shawangunk Formation. The Shawangunk Formation decreases in thickness from 600 m at the Delaware Water Gap, Pennsylvania to its pinchout at Rosendale, New York (Epstein and Lyttle, 1987). It unconformably overlies black shales of the Ordovician-aged Martinsburg Formation, and is overlain by Late Silurian- to Middle Devonian-aged carbonate rocks. The Shawangunk Formation consists of orthoquartzitic, thickly bedded, well indurated, medium- to coarse-grained sandstones and conglomerates. The rocks were diagenetically silicified prior to faulting (Wilbur et al., 1990) making them well suited to being idealized as a continuous medium. This lithology provides a generally isotropic medium containing ample microfractures which are suitable for demarcating the process zones resulting from fault growth (Vermilye and Scholz, 1998).

3. Procedure

Several faults along the Shawangunk ridge were mapped in detail and oriented samples were examined in the laboratory. Mossy Maple fault was one of five of these faults, used to develop the fault process zone model of Vermilye and Scholz (1998). This fault was selected for more detailed analysis owing to the simplicity of the fault tip geometry and because preliminary microfracture orientations showed a mode II signature, which indicates propagation direction of the fault tip. Local macrostructural data were recorded and additional samples were collected in order to investigate propagation directions associated with fault segmentation. Three mutually perpendicular thin sections were produced from four of the samples, with one of the three sections cut perpendicular to the fault plane and parallel to the slip direction. This orientation best reveals fault-related microfractures (Engelder, 1974). Observations showed that measurements made only on slides of this orientation produce a good representation of measurements made by combining data from all three orientations (Vermilye and Scholz, 1998). Reducing observations to one thin section for each location allowed examination of more locations along the fault.

Microfracture densities were measured by counting the number of microfractures intersecting a 0.39 mm transect across a quartz grain at 250 × . Densities are reported as the number of microfractures per mm (mf/mm). Two perpendicular transects were made for each grain in order to eliminate bias resulting from the orientation of the transect. While grains were ran-

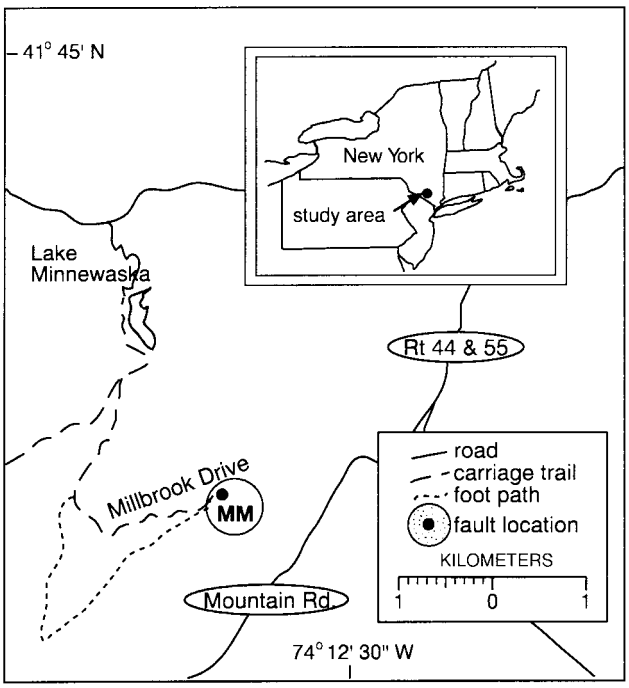

Fig. 2. Map of field location (inset) and fault location along the Shawangunk ridge, Ulster County, New York. MM represents location of Mossy Maple fault (after Vermilye and Scholz, 1998).

domly selected, those with diameters smaller than the transect length were rejected. Density counts were made on at least 10 grains for each thin section and an average density was computed for the location.

Microstructure orientations were measured on a universal stage microscope. We attempted to reduce operator bias (Borg et al., 1960) by making observations with maximum angular sweeps, looking for features at high angles to the viewing direction. To ensure a statistically significant population, at least one hundred microfracture orientation measurements were made on each thin section (Anders and Wiltschko, 1994) when possible. The resulting data were rotated from the thin section reference frame back to geographical coordinates. Measurements were plotted on equal area stereonets and contoured using the Kamb method (Kamb, 1959). A Bingham axial distribution analysis was used to determine the orientation of the maximum microfracture density for each location (Cheeney, 1983).

Fault core thicknesses were determined in three ways. On each thin section, core thickness was measured for at least four locations and an average thickness was calculated for the sample location along the fault trace. The thickness of a macroscopically observed mineralized zone was also measured on the cores with dial calipers. For one location (between cores 1 and 10) the mineralized zone was measurable in the field. Since no sample was taken at this location a core zone thickness was calculated utilizing the observed ratio between core zone thickness and the thickness of the mineralized zone (1:2).

4. Observations

Mossy Maple fault is located on Millbrook Mountain in Minnewaska State Park, Gardiner, NY (Fig. 2). This strike-slip fault intersects the cliff face 40 m south of the end of Millbrook Drive. The fault trace is exposed in both a near vertical cliff face and along the gently dipping cliff-top bedding surface. Both exposures include a fault tip. From the cliff edge, the fault tips are located 6.7 m along strike and 3.6 m down dip. The strike azimuth for the main body of the fault is 294° and changes to 333° at the northern tip (Fig. 3). Dips are sub-vertical but at segment ends, adjacent segment tips dip towards one another, suggesting that they intersect below the outcrop surface. Exposed slickenlines show bedding-parallel slip, with the orientation of secondary faults (Petit, 1987) and the orientation of pressure solution cleavage planes indicating right-lateral slip. Displacements measured from offset conglomerate pebbles are between 1.5 and 6 cm. The lack of abundant pre-existing markers precludes a more detailed assessment of displacements.

This study was done on a fully exposed section of the horizontal trace extending 2.26 m from the NW fault tip. This section is composed of three distinct, closely aligned segments. The general orientation for the strike azimuth of all three segments is 294°, with a change in orientation of the terminal 100 mm of the northern most segment to 333°. In addition to two oriented hand samples, a series of 14 cores was drilled along the fault trace and in the vicinity of the fault,

Fig. 3. Mossy Maple fault outcrop map and microfracture orientations. The slip direction is indicated by half-arrows along the fault. Open circles with sample identification numbers represent sample locations. For all equal area stereoplots the plane of the projection is horizontal and in geographical coordinates. Poles to microfractures are contoured using the Kamb (1959) method. Three standard deviations are considered a uniform distribution and the contour interval is two standard deviations. The orientation of the maximum concentration is represented by the dashed great circle for samples along the fault. The orientations of maximum concentrations for background microfracture populations from samples MM14 and MMS1 are plotted as the dotted great circles and also plotted for reference in all other stereoplots. The solid great circle represents the local fault orientation for each sample location. Above or below each stereoplot are the sample number, fault = the local fault orientation, mfc = the mean microfracture orientation, angle = the angle between the local fault orientation and the mean microfracture orientation, and N = the number of microfractures measured.

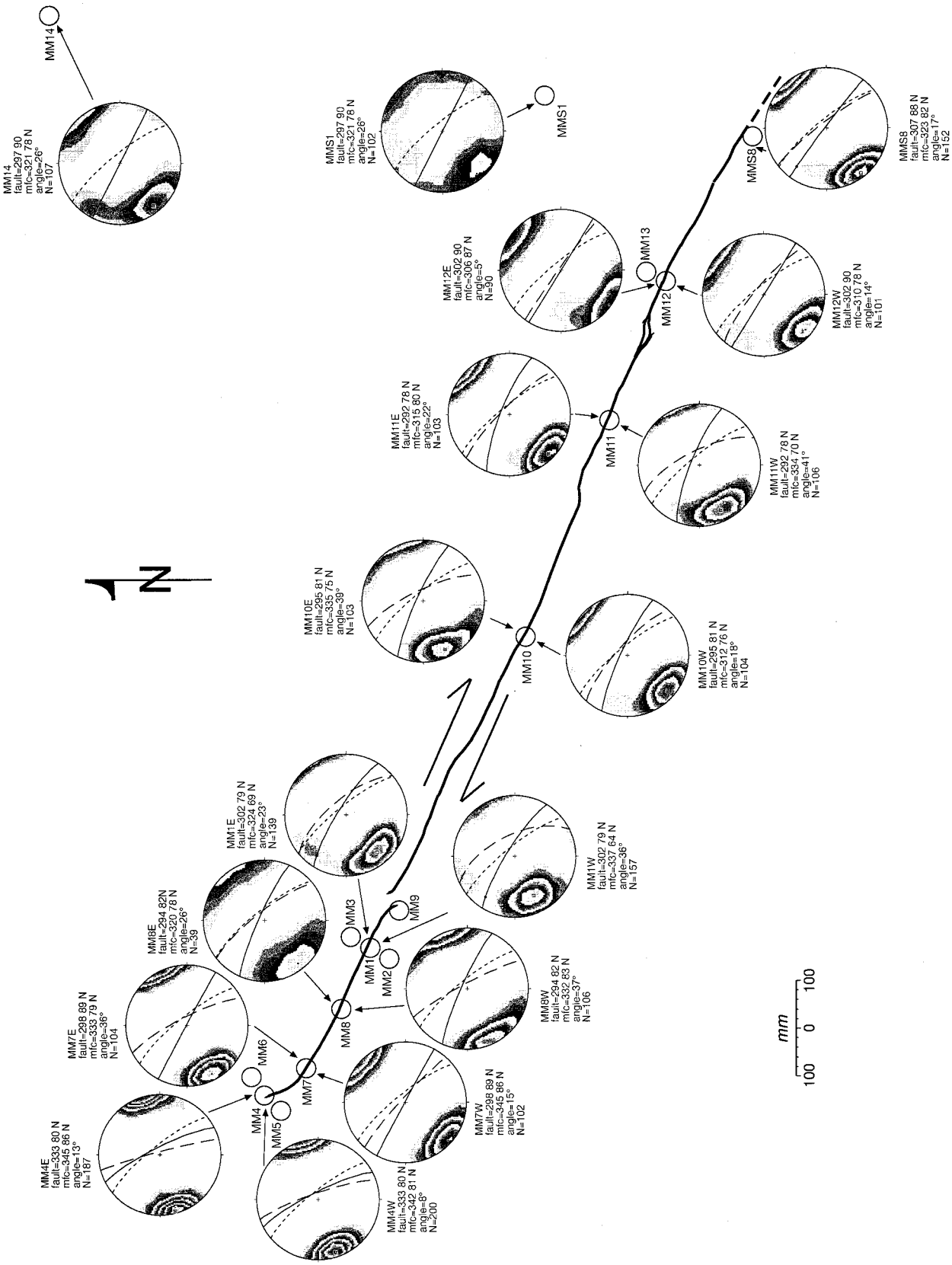
MM14
MM14
fault=297 90
mfc=321 78 N
angle=26°
N=107
MMS1
MMS1
fault=297 90
mfc=321 78 N
angle=26°
N=102
MMS8
MMS8
fault=307 88 N
mfc=323 82 N
angle=17°
N=152
MM13
MM12E
fault=302 90
mfc=306 87 N
angle=5°
N=90
MM12
MM12W
fault=302 90
mfc=310 78 N
angle=14°
N=101
MM11E
fault=292 78 N
mfc=315 80 N
angle=22°
N=103
MM11
MM11W
fault=292 78 N
mfc=334 70 N
angle=41°
N=106
MM10E
fault=295 81 N
mfc=335 75 N
angle=39°
N=103
MM10
MM10W
fault=295 81 N
mfc=312 76 N
angle=18°
N=104
N
MM1E
fault=302 79 N
mfc=324 69 N
angle=23°
N=139
MM1W
fault=302 79 N
mfc=337 64 N
angle=36°
N=157
MM3
MM9
MM1
MM2
MM8E
fault=294 82N
mfc=320 78 N
angle=26°
N=39
MM8W
fault=294 82 N
mfc=332 83 N
angle=37°
N=106
MM8
MM7E
fault=298 89 N
mfc=333 79 N
angle=36°
N=104
MM6
MM7
MM7W
fault=298 89 N
mfc=345 86 N
angle=15°
N=102
MM4
MM5
MM4E
fault=333 80 N
mfc=345 86 N
angle=13°
N=187
MM4W
fault=333 80 N
mfc=342 81 N
angle=6°
N=200
mm
100 0 100

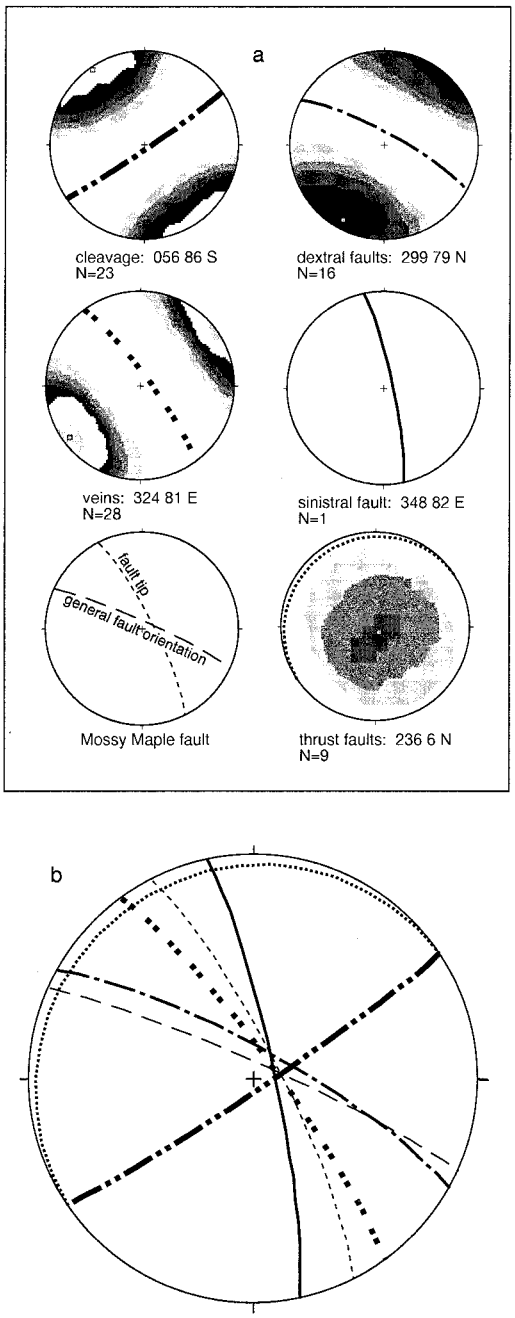

Fig. 4. Milbrook Mountain structural data from field measurements. (a) Stereoplots of contoured poles to: pressure solution cleavage planes, dextral faults, extensional veins, thrust faults, and the best-fit plane for each structure. The orientation of the best-fit plane and N = number of structures are shown below each plot. Also shown are a single sinistral fault orientation and the orientation for Mossy Maple fault. (b) The best-fit plane for each structure and the orientation of Mossy Maple fault are plotted using the distinctive line types from (a) (see caption to Fig. 3 for description of contouring procedure).

including two control samples well away from the fault. Fig. 3 shows a map view of the fault trace and sample locations. The two separate parts of cores, cut by the fault, are differentiated with an E or W added to the sample number, indicating a location on the east or west side of the fault.

Macrostructural data were collected at the Mossy Maple outcrop and adjacent outcrops in order to better understand the local structural context. Orientations for thrust, right- and left-lateral slip faults are shown in Fig. 4(a), along with the orientations for pressure solution cleavage planes and quartz-filled extension veins. The best-fit pole for each data set was calculated and the corresponding planes are plotted in Fig. 4(b). The orientation for Mossy Maple fault and the orientation of the NW fault tip are shown for comparison in Fig. 4(a) and (b). Fault trace lengths are of the order of meters to tens of meters while vein trace lengths are an order of magnitude smaller. The veins are localized in clusters while the faults are more evenly distributed. Cross-cutting relations indicate that the structures are coeval.

Examination of the cores shows a discrete planar fault with polished slip surfaces and well developed slickenlines on all but two samples (cores MM4 and MM12). The fracture surface in core MM4, containing the fault tip, is rough with interlocking grains and shows no striae. The surface in core MM12 has grooves indicating shear displacement but lacks the polished surface and well developed striae observed in other cores. The fault surface in all cores is contained within a lighter colored mineralized zone, which extends a few millimeters into the wall rock. The fault plane is not centrally located within the fault core. It is located closer to one side, but not consistently the same side. Thirty-three thin sections were made for examination of microscopic structures. Inspection showed abundant healed microfractures, defined by aligned fluid inclusions or mineral precipitates, as well as microveins. The microveins are quartz-filled and roughly two orders of magnitude wider than the microfractures, with apertures of the order of 0.1 mm. Deformation lamellae and pressure solution structures were also observed.

Healed microfractures are the dominant microscopic deformation structures. Background samples taken 375 mm (sample MMS1) and 1.4 m northeast of the fault (MM14) have microfracture densities of 14 and 15 mf/mm, respectively. This is consistent with other Shawangunk Formation background microfracture densities of 13, 14 and 17 mf/mm (Vermilye and Scholz, 1998). The background microfracture orientations indicate the greatest compressive stress at 26° from the fault at both locations and they are consistent with the macroscopically observed right-lateral sense of slip. This direction is normal to the strike of the regional folds and thrusts and is consistent with field observations that the strike-slip faulting is coeval with the major contractional structures in the area. The implied greatest compressive stress is also consistent

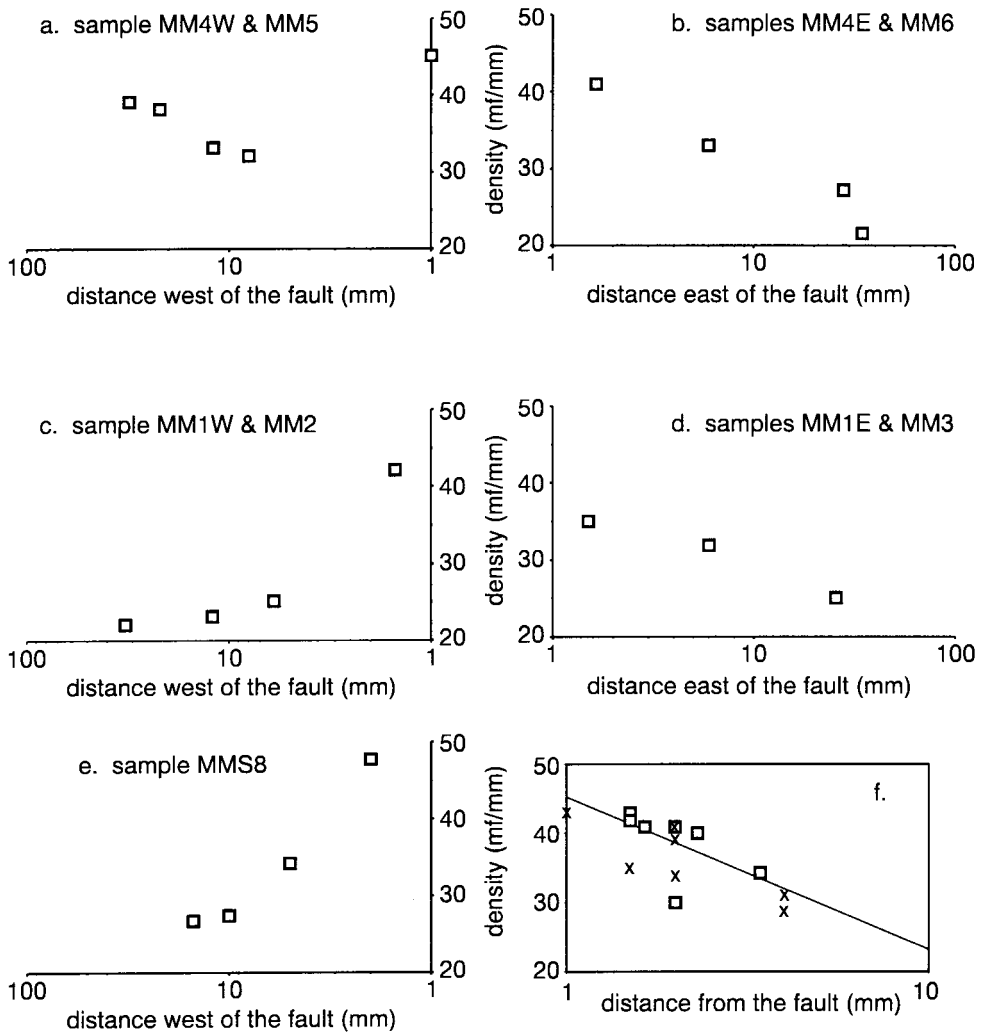

Fig. 5. Microfracture density–distance plots for Mossy Maple fault. Density is recorded as the number of microfractures per millimeter (mf/mm) and is plotted relative to distance from the fault plane, for both sides of the fault in (a and b) and (c and d) and one side of the fault in (e). In plot (f) the squares represent microfracture densities from the dilational quadrants along the fault and crosses represent densities from compressional quadrants.

with all macroscopic structures shown in Fig. 4. The microfracture density increases logarithmically with proximity to the fault plane (Fig. 5b–f). These increases in density are similar to the logarithmic increases observed for several other Shawangunk faults (Vermilye and Scholz, 1998). Sample MM5 (Fig. 5a), which shows an increase in density from 10 to 30 mm west of the fault trace, is collinear with the general fault orientation, along strike northwest of sample MM7 (Fig. 3).

The increase in density is accompanied by a change in microfracture orientations. For most cores there is a distinct asymmetry of orientations across the fault plane. Samples MM1W, MM7E, MM8W, MM10E, and MM11W contain microfractures at higher angles to the fault than the background microfracture population and samples MM1E, MM7W, MM10W and MM11E show microfractures at lower angles. This asymmetry across the fault plane is the signature of mode II fracture propagation, indicating dilational and compressional quadrants, and the direction of propagation past the point of observation. The sense of asymmetry is variable along the fault trace implying changes in the propagation direction. Microfracture densities from dilational quadrants and compressional quadrants are plotted separately in Fig. 5(f), with squares representing dilational quadrants and crosses representing compressional quadrants. Densities for six of seven dilational quadrants plot above the line representing the best-fit logarithmic function. Five of seven compressional quadrant densities plot below the line, indicating that densities in the dilational quadrants are generally higher. This observation is similar to previous field and laboratory results (Reches and

Lockner, 1994; Moore and Lockner, 1995; Vermilye and Scholz, 1998).

Cores MM4 and MM12 have microfracture populations that are more symmetric across the fault and form lower angles with the local fault plane than microfractures in the background sample. The maximum microfracture concentrations for core MM4 are 8° from the fault on the west side of the fault and 13° on the east side. Microfracture concentrations for core MM12 are at 14° from the fault on the southwest side of the fault and 4° from the fault on the northeast side. Fracture-parallel microfractures indicate mode I propagation. This implied change in propagation mode for core 4 is consistent with the lack of shear displacement, cataclasite development, or slickenlines on the fracture surface. While core MM12 displays

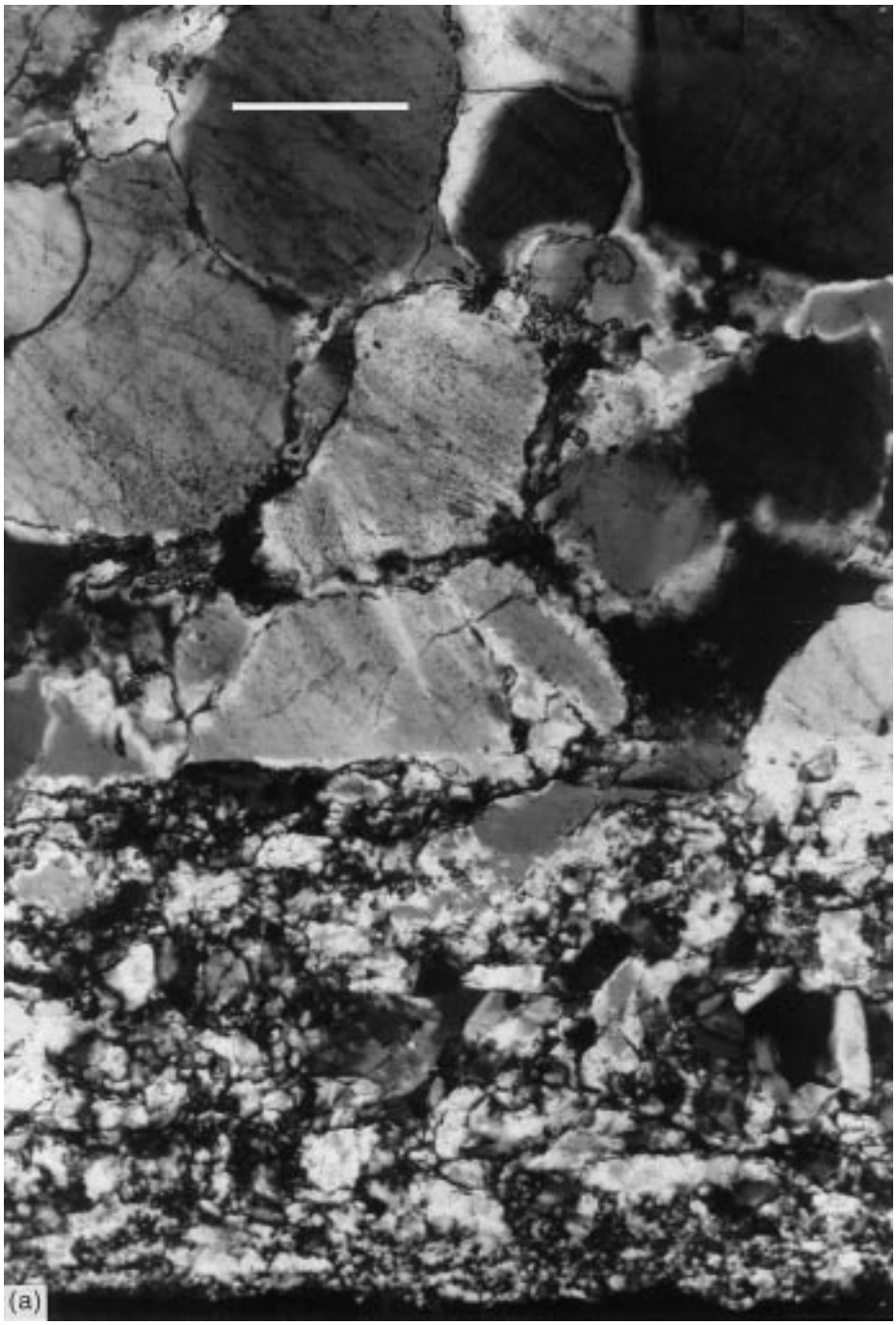

Fig. 6. (a) Photomicrograph of the fault surface (bottom), cataclasite zone (fine grained material just adjacent to fault surface) and process zone (microfractured quartz grains above cataclasite). The scale bar is 0.5 mm in length. (b) Photograph showing the bifurcation of a fault plane around a lozenge of more resistant material. The pen is parallel to the slip direction. The scale bar is 10 cm in length.

Fig. 6 (*continued*)

development of a fault core and grooves indicating shear displacement, the fault surface is more irregular than in other cores and lacks slickenlines. This may indicate mode I propagation followed by shearing displacement.

The fault core is made up of cataclasite. This fine-grained quartz, showing evidence of fracturing, rotation and induration, has a well defined boundary with the wall rock in some locations (Fig. 6a) but generally wall rock grains project into the finer grained material, forming a layer of non-uniform thickness. Multiple measurements were made for each sample and the average thicknesses show an increase with distance from the tip of each segment boundary (Fig. 7). The slip plane location within the cataclasite varies, but not randomly. It is always closer to the interface with the dilational quadrant as defined by the microfracture orientations. This location suggests that the shear surface moves into more densely microfractured material along that boundary.

5. Interpretation

The surface trace and the variations in fault core thickness indicate that this section of the fault is composed of three distinct segments, labeled A, B and C in Fig. 7. Since gouge thickness scales with fault slip (Scholz, 1987; Hull, 1988), by analogy we expect thickness of the cataclasite to increase with slip also. It is therefore reasonable to assume that slip initiated on segments A and B near the segment centers. Moreover, we suggest that the microfracture patterns along the fault trace represent the process zone, left as a wake behind the propagating tip and that they indicate bilateral propagation of the fracture from the centers of both segments (Fig. 8). These data could be interpreted as evidence for independent nucleation and linkage of initially isolated fault segments. However, we suggest an alternative interpretation.

Consideration of the three-dimensional nature of fault planes suggests a more likely interpretation, in which segmentation results from uneven propagation

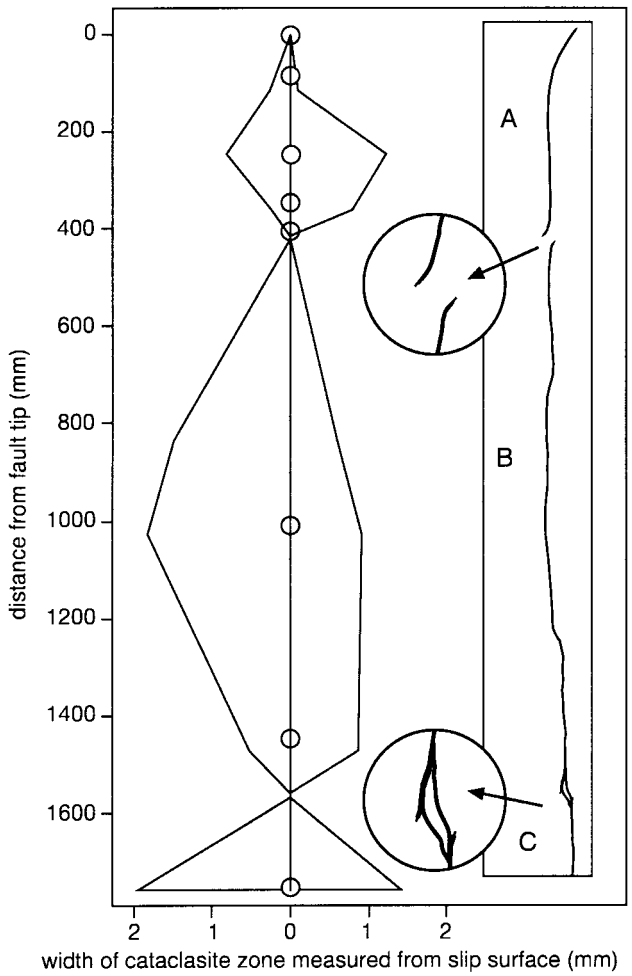

Fig. 7. Plot of cataclasite layer thickness relative to distance from the fault tip. The origin represents the slip plane. Inset shows fault trace with segments labeled and boundaries enlarged.

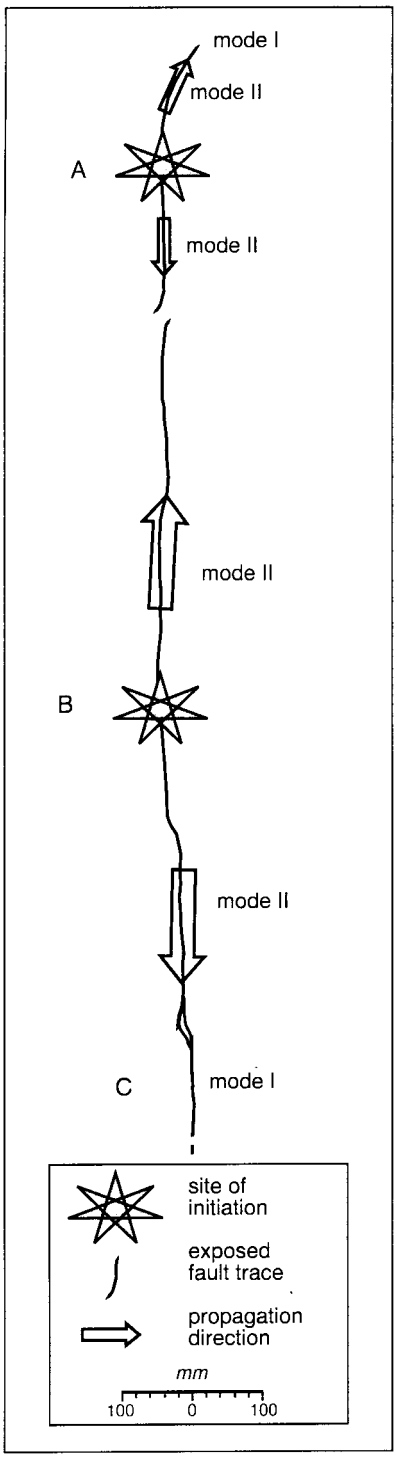

Fig. 8. Interpretation of propagation directions for fault segments based on microfracture orientations.

of a single fault tip as it encounters a volume of more resistant rock. While Mossy Maple fault lacks a well exposed slip surface, a nearby strike-slip fault surface is well-exposed, and on this fault plane we observed a location where a lozenge of more resistant material caused the fault to bifurcate, forming two segments, on opposite sides of the lozenge (Fig. 6b). We propose a similar origin for the segmentation of Mossy Maple fault. In our model segment B is propagating northwest as a mode II fracture and encounters a mass of resistant material. Below and above the obstacle the fault plane continues to propagate in the same plane, but at the obstacle the fracture tip is deflected out-of-plane impeding continued propagation. The fracture is pinned in the region of the obstacle but propagates around it to near the center of segment A and then out toward the tips of the segment (Fig. 9). While the details of slip are quite different for dislocations, for the purpose of visualization, this process is analogous to a Frank–Read dislocation source (Suppe, 1985, fig. 4-13). Huggins et al. (1995, fig. 13) propose a similar scenario for fault segmentation though with fewer constraints, since they did not measure the propagation directions, a key element in our reconstruction of events. In our interpretation the overall unilateral

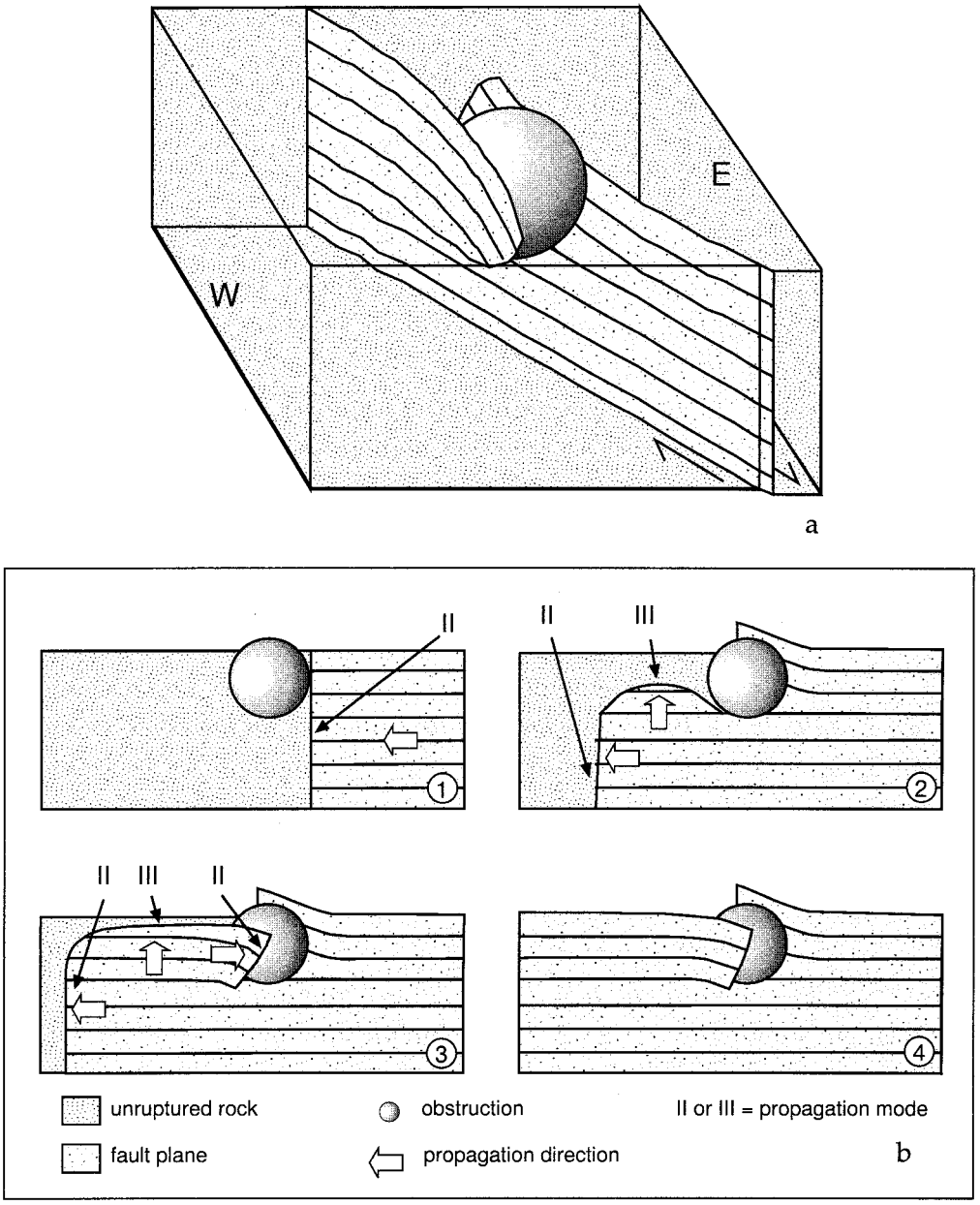

Fig. 9. Our model of segmentation resulting from uneven propagation of the fault tip as it encounters a volume of rock with a higher fracture toughness.

propagation of the fault is interrupted at segment boundaries where bilateral propagation accommodates slip around obstacles.

Silicification of the Shawangunk Formation produced highly indurated rock in which the quartz cement appears in most cases to have eliminated grain boundary weakness along the sand grains and conglomerate clasts. The rock material located within both Mossy Maple segment boundaries and the lozenge of material shown in Fig. 6(b) show evidence of intense pressure solution deformation. In all cases the combination of dextral displacement and left-stepping geometry result in compressional segment boundaries, where dissolution has altered the material properties of the rock, presumably subsequent to propagation of the fault. The present day material properties of these rock masses are not expected to represent the pre-faulting properties. As such we do not have material evidence confirming that resistant material existed at segment boundaries before fault propagation. The fault geometry and microfracture populations are consistent with the hypothesis that resistant masses were present during propagation.

The two samples displaying mode I fracture propagation are located within 100 mm of the fault tip and at the tip of segment C. We interpret this as evidence

for mode I propagation as part of the fault growth process, even within a compressional environment. This is not surprising, because the roughness of the fault surface requires some opening mode displacement in order to accommodate shearing. This suggests that at those locations, where shear displacement is small, the mode I component dominates in producing microfractures. This may occur either during fault propagation or after the release of compressive stresses during unroofing. The orientations of the tips are rotated toward σ_1 relative to the orientation of the main body of the fault. This represents propagation of the fault tip and segment tips into the macroscopic dilational quadrants in both cases and is consistent with laboratory and field observations (e.g. Petit and Barquins, 1988; McGrath and Davison, 1995). We suggest that the mode I tips may have formed as release fractures, subsequent to faulting. We propose that release fractures form when unroofing releases tensile stresses stored in the cataclasite zone. The tensile stresses result from dilation of rock material during cataclasite formation but are of insufficient magnitude to drive local mode I fracture while the fault remains at high confining pressure at depth. This interpretation is consistent with the orientation of the fault plane and the microfracture orientations and may explain the elevated density in core MM5 (beyond MM7 and colinear with the general fault trace) as damage resulting from the fault tip, prior to formation of the release fracture.

6. Discussion

Our interpretation for the growth of Mossy Maple fault is based on observations of process zones along several small faults in the Shawangunk Mountains. An alternative interpretation is that Mossy Maple did not propagate as a fault, but grew within an earlier stress field as an opening-mode vein or veins, which were later reactivated as a fault under a different stress field. This model has been developed to explain the growth of small, brittle faults in granodiorite of the Sierra Nevada in California (Segall and Pollard, 1983) and a comparison of the two models of fault growth, relative to Mossy Maple fault follows.

The field scale structures in the Shawangunk Formation show no indication of an earlier stress field. The orientations of the opening-mode veins are consistent with formation within the same stress field as the faults and pressure solution cleavage (Fig. 4). In the Sierran outcrops, the faults and veins are parallel. The dilational fractures located at the ends of the Sierran faults formed parallel to the maximum compressive stress inferred for the faulting, not the compressive stress inferred for vein formation (Segall and Pollard, 1983). This is consistent with their model of the faults as reactivated veins, resulting from rotation of the stress field. Dissimilarly, the dilational fracture located at the tip of segment A, in Mossy Maple fault is parallel to outcrop scale veins, consistent with formation within the same stress field. While the hooked geometries observed at Mossy Maple segment boundaries look similar to overlapping joint boundaries (Olson and Pollard, 1989; Cruikshank et al., 1991), stress field analyses (Segall and Pollard, 1980) show that stress fields for interacting faults can also produce hooked geometries.

Stress concentrations associated with the propagating tips of opening-mode fractures have been observed to produce process zones analogous to the process zones associated with faults (Delaney et al., 1986; Pollard and Segall, 1987). Within these process zones the fracturing is not asymmetric across the propagating fracture as in faulting, but fractures form parallel to the propagating joint or dike (Pollard and Segall, 1987). If Mossy Maple fault had grown as a joint, we might expect to see fault-parallel microfractures along the fault trace, overprinted by microfractures associated with the faulting. Fault-parallel microfractures at the fault tip (sample MM4) are not parallel to the general fault orientation, and therefore do not represent an earlier, joint associated process zone. The microfractures from sample MM12 are subparallel to the fault and could be interpreted as evidence for joint propagation in an earlier stress field. The lack of fault-parallel microfractures at all the other sampling locations does not support this interpretation. We prefer the interpretation that microfractures in sample MM12 represent localized opening-mode propagation contemporaneous with shear propagation, since the vast majority of the microfractures along the fault trace form populations that are asymmetrically distributed across the fault. While our observations do not demonstrate unequivocally that Mossy Maple fault formed as a fault as opposed to a joint, both the field and microstructural data are more consistent with a fault growth origin.

7. Conclusions

We have examined the fault trace, the process zone and cataclasite zone of a small, brittle fault. The dominant microscopic deformation structures are healed tensile microfractures. There is a low density background microfracture population with a mean microfracture orientation perpendicular to the least compressive stress (σ_3) implied by the structural trends observed in the field. The associated greatest compressive stress (σ_1) forms an acute angle with the small strike-slip fault examined in this study. We interpret

the mean orientation of these background microfractures to represent the orientation of the remote σ_1, unaltered by faulting.

The microfractures show a logarithmic increase in density as a function of proximity to the fault plane. We consider the volume of rock in which the microfracture density exceeds the general background microfracture density, to delineate the process zone. The process zone microfractures in most of the cores are consistent with formation within the altered stress fields of propagating mode II fault tips. They are asymmetrically distributed with respect to the fault plane. They form higher angles with the fault plane than the background population on one side of the fault and lower angles on the opposite side. The sense of asymmetry is not consistent along the fault trace but alternates at segment centers and one of the segment boundaries. We interpret the alteration in sense of asymmetry to represent changes in propagation directions, indicating growth of individual segments from the centers toward the tips. Growth of segments from the centers outward is consistent with maximum cataclasite layer thickness in the segment centers. We propose a scenario for the growth history of this fault in which the observed segmentation results from uneven propagation of the fault tip as it encounters masses of more resistant rock.

Acknowledgements

We would like to thank Mark Anders, Nick Christie-Blick and Roy Schlische for helpful comments and reviews of this manuscript. The study would not have been possible without access to the fault location provided by Minnewaska New York State Park. The stereographic projections were made with the 'Stereonet' program written by R.W. Allmendinger. Stephen Martel and an anonymous reviewer provided detailed reviews which led to substantial improvements in the paper. This work was supported by a research grant from GSA and NSF grant #EAR 94-05326. Lamont–Doherty Earth Observatory contribution 5933.

References

Anders, M.H., Schlische, R.W., 1994. Overlapping faults, intrabasin highs, and the growth of normal faults. Journal of Geology 103, 165–180.

Anders, M.H., Wiltschko, D.V., 1994. Microfracturing, paleostress and the growth of faults. Journal of Structural Geology 16, 795–815.

Beaumont, C., Quinlan, G.M., Hamilton, J., 1987. The Alleghanian orogeny and its relationship to the evolution of the eastern interior, North America. In: Beaumont, C., Tankard, A.J. (Eds.), Sedimentary Basins and Basin-Forming Mechanisms, Memoir 12. Canadian Society of Petroleum Geologists, pp. 425–445.

Berkey, C.P., 1911. The geology of the New York aqueduct. New York State Museum Bulletin 146, 55–66.

Borg, I.Y., Friedman, M., Handin, J., Higgs, D.V., 1960. Experimental deformation of St. Peter Sand: A study of cataclastic flow. Memoirs of the Geological Society of America 79, 133–171.

Burgmann, R., Pollard, D.D., 1994. Strain accommodation about strike-slip fault discontinuities in granitic rock under brittle-to-ductile conditions. Journal of Structural Geology 16, 1655–1674.

Burgmann, R., Pollard, D.D., Martel, S.J., 1994. Slip distributions on faults: effects of stress gradients, inelastic deformation, heterogeneous host-rock stiffness, and fault interaction. Journal of Structural Geology 16, 1675–1690.

Caine, J.S., Evans, J.P., Forster, C.B., 1996. Fault zone architecture and permeability structure. Geology 24, 1125–1128.

Cartwright, J., Trudgill, B.D., Mansfield, C.S., 1995. Fault growth by segment linkage: An explanation for scatter in maximum displacement and trace length data from the Canyonlands Grabens of SE Utah. Journal of Structural Geology 17, 1319–1326.

Cheeney, R.F., 1983. Statistical Methods in Geology. George Allen & Unwin, London.

Cowie, P.A., Scholz, C.H., 1992. Physical explanation for displacement–length relationship of faults using a post-yield fracture mechanics model. Journal of Structural Geology 14, 1133–1148.

Cox, S.J.D., Scholz, C.H., 1988a. Rupture initiation in shear fracture of rocks: an experimental study. Journal of Geophysical Research 93, 3307–3320.

Cox, S.J.D., Scholz, C.H., 1988b. On the formation and growth of faults: an experimental study. Journal of Structural Geology 10, 413–430.

Cruikshank, K.M., Zhao, G., Johnson, A.M., 1991. Analysis of minor fractures associated with joints and faulted joints. Journal of Structural Geology 13, 865–886.

Dawers, N.H., Anders, M.H., 1995. Displacement–length scaling and fault linkage. Journal of Structural Geology 17, 607–614.

Delaney, P.T., Pollard, D.D., Ziony, J.I., McKee, E.H., 1986. Field relations between dikes and joints: emplacement processes and paleostress analysis. Journal of Geophysical Research 91, 4920–4938.

Engelder, J.T., 1974. Cataclasis and the generation of fault gouge. Geological Society of America Bulletin 85, 1515–1522.

Engelder, J.T., Fischer, M.P., Gross, M.R., 1993. Geological aspects of fracture mechanics, short course manual prepared for Annual Meeting, Geological Society of America, Boston, Massachusetts.

Epstein, J.B., Lyttle, P.T., 1987. Structure and stratigraphy above, below, and within the Taconic unconformity, southeastern New York. In: Waines, R.H. (Ed.), New York State Geological Association 59th Annual Meeting, Kingston, New York, November 6–8, 1987 Field Trip Guidebook. New Paltz, N.Y. State University, New York, pp. C1–C78.

Friedman, M., Handin, H., Alani, 1972. Fracture surface energy in rocks. International Journal of Rock Mechanics, Mineral Science and Geomechanical Abstracts 8, 757–766.

Hallbauer, D.K., Wagner, H., Cook, N.G.W., 1973. Some observations concerning the microscopic and mechanical behavior of quartzite specimens in stiff, triaxial compression tests. International Journal of Rock Mechanics, Mineral Science and Geomechanical Abstracts 10, 713–726.

Huggins, P., Watterson, J.J., Walsh, J.J., Childs, C., 1995. Relay zone geometry and displacement transfer between normal faults recorded in coal-mine plans. Journal of Structural Geology 17, 1741–1755.

Hull, J., 1988. Thickness–displacement relationships for deformation zones. Journal of Structural Geology 10, 431–435.

Ingraffea, A.R., 1987. Theory of crack initiation and propagation.

In: Atkinson, B. (Ed.), Fracture Mechanics of Rock. Academic Press, London.

Kamb, B., 1959. Ice petrofabric observations from the Blue Glacier, Washington, in relation to theory and experiment. Journal of Geophysical Research 64, 1891–1909.

Lakatos, S., Miller, D.S., 1983. Fission-track analysis of apatite and zircon defines a burial depth of 4 to 7 km for lowermost Upper Devonian, Catskill Mountains, New York. Geology 11, 103–104.

Lawn, B.R., Wilshaw, T.R., 1975. Fracture of Brittle Solids. Cambridge University Press, New York.

Lockner, D.A., Byerlee, J.D., Kuksenko, V., Ponomarev, A., Sidorin, A., 1991. Quazi-static fault growth and shear fracture energy in granite. Nature 350, 39–42.

Lockner, D.A., Moore, D.E., Reches, Z., 1992. Microcrack interaction leading to shear fracture. In: Rock Mechanics, Proceedings of the 33rd US Symposium. A.A. Balkema, Rotterdam, pp. 807–816.

Martel, S.J., Pollard, D.D., Segall, P., 1988. Development of simple strike-slip fault zones, Mount Abbot Quadrangle, Sierra Nevada, California. Geological Society of America Bulletin 100, 1451–1465.

McGrath, A.G., Davison, I., 1995. Damage zone geometry around fault tips. Journal of Structural Geology 17, 1011–1024.

Moore, D.E., Lockner, D.A., 1995. The role of microfracturing in shear-fracture propagation in granite. Journal of Structural Geology 17, 95–114.

Olson, J., Pollard, D.D., 1989. Inferring paleostress from natural fracture patterns: a new method. Geology 17, 345–348.

Peacock, D.C.P., 1991. Displacements and segment linkage in strike-slip fault zones. Journal of Structural Geology 13, 1025–1035.

Peacock, D.C.P., Sanderson, D.J., 1991. Displacements, segment linkage and relay ramps in normal fault zones. Journal of Structural Geology 13, 721–733.

Peacock, D.C.P., Sanderson, D.J., 1994. Geometry and development of relay ramps in normal fault systems. American Association of Petroleum Geologists Bulletin 78, 147–165.

Petit, J.P., 1987. Criteria for sense of movement on fault surfaces in brittle rocks. Journal of Structural Geology 9, 597–608.

Petit, J.P., Barquins, M., 1988. Can natural faults propagate under mode II conditions? Tectonics 7, 1243–1256.

Pollard, D.D., Segall, P., 1987. Theoretical displacements and stresses near fractures in rock: With applications to faults, joints, veins, dikes, and solution surfaces. In: Atkinson, B. (Ed.), Fracture Mechanics of Rock. Academic Press, San Diego, California, pp. 277–349.

Reches, Z., Lockner, D.A., 1994. Nucleation and growth of faults in brittle rocks. Journal of Geophysical Research 99, 18159–18173.

Scholz, C.H., 1968. Microfracturing and the inelastic deformation of rock in compression. Journal of Geophysical Research 73, 1417–1432.

Scholz, C.H., 1987. Wear and gouge formation in brittle faulting. Geology 15, 493–495.

Scholz, C.H., Dawers, N.H., Yu, J.Z., Anders, M.H., Cowie, P.A., 1993. Fault growth and fault scaling laws: preliminary results. Journal of Geophysical Research 98, 21951–21961.

Segall, P., Pollard, D.D., 1980. Mechanics of discontinuous faults. Journal of Geophysical Research 85, 555–568.

Segall, P., Pollard, D.D., 1983. Nucleation and growth of strike slip faults in granite. Journal of Geophysical Research 88, 4337–4350.

Suppe, J., 1985. Principles of Structural Geology. Prentice-Hall, Englewood Cliffs, New Jersey.

Trudgill, B., Cartwright, J., 1994. Relay ramp forms and normal fault linkages, Canyonlands National Park, Utah. Geological Society of America Bulletin 106, 1143–1157.

Vermilye, J.M., Scholz, C.H., 1998. The process zone: A microstructural view of fault growth. Journal of Geophysical Research 103, 12223–12237.

Wilbur, J.S., 1986. Shawangunk Mountains, New York zinc–lead–copper veins: Fluid inclusions, geochemical, and isotope studies. Masters thesis, Eastern Washington University.

Wilbur, J.S., Mutschler, F.E., Friedman, J.D., Zartman, R.E., 1990. New chemical, isotopic, and fluid inclusion data from zinc–lead–copper veins, Shawangunk Mountains, New York. Economic Geology 85, 182–196.